ELSEVIER

NeuroImage

www.elsevier.com/locate/ynimg
NeuroImage 25 (2005) 942–951

Spatiotemporal brain dynamics in response to muscle stimulation

David M. Niddam,[a,b,c,d] Li-Fen Chen,[a,b,c,d] Yu-Te Wu,[c,d,e] and Jen-Chuen Hsieh[a,b,c,d,f,g,*]

[a]*Center for Neuroscience, National Yang-Ming University, Taipei, Taiwan*
[b]*Faculty of Medicine, School of Medicine, National Yang-Ming University, Taipei, Taiwan*
[c]*Laboratory of Integrated Brain Research, Department of Medical Research and Education, Taipei Veterans General Hospital, Taipei, Taiwan*
[d]*Brain Research Center—National Yang-Ming University, University System of Taiwan, Taipei, Taiwan*
[e]*Institute of Radiological Science, National Yang-Ming University, Taipei, Taiwan*
[f]*Institute of Health Informatics and Decision Making, School of Medicine, National Yang-Ming University, Taipei, Taiwan*
[g]*Institute of Neuroscience, School of Life Science, National Yang-Ming University, Taipei, Taiwan*

Received 18 August 2004; revised 19 November 2004; accepted 2 December 2004
Available online 10 February 2005

The objective of the present study was to assess the spatiotemporal scenario of brain activity associated with sensory stimulation of the abductor pollicis brevis muscle. Spatiotemporal dipole models, using realistic individual boundary element head models, were built from somatosensory evoked potentials (SEPs; 64 Ch. EEG) to nonpainful and painful intramuscular electrostimulation (IMES) as well as to cutaneous electrostimulation delivered to the distal phalanx of the thumb. Nonpainful and painful muscle stimuli resulted in activation of the same brain regions. In temporal order, these were: the contralateral primary sensorimotor cortex, contralateral dorso-lateral premotor area (PM), bilateral operculo-insular cortices, caudal cingulate motor area (CMA), and posterior cingulate cortex/precuneus. Brain processing induced by muscle sensory input showed a characteristic pattern in contrast to cutaneous sensory input, namely: (1) no early SEP components to IMES; (2) an initial IMES component likely generated by proprioceptive input is not present for digit stimulation; (3) one source was located in the PM only for IMES. This source was unmasked by the lower stimulus intensity; (4) a source for IMES was located in the contralateral caudal CMA rather than being located in the cingulate gyrus. Cerebral sensory processing of input from the muscle involved several sensory and motor areas and likely occurs in two parallel streams subserving higher order somatosensory processing as well as sensory–motor integration. The two streams might on one hand involve sensory discrimination via SI and SII and on the other hand integration of sensory feedback for further motor processing via MI, lateral PM area, and caudal CMA.

Keywords: Intramuscular electrostimulation; SEP; Source localization; Realistic head model; Pain

Introduction

The majority of brain imaging studies on the processing of sensory input from muscle have been concerned with proprioception. Only a few studies have investigated the processing of muscle stimuli originating from other sensory modalities. In fact, the majority of sensory receptors in skeletal muscles originate from smaller afferents (Abrahams, 1986). One way to elicit responses from sensory fibers within the muscle is by nonspecific intramuscular electrostimulation (IMES). Ideally, the population of afferents recruited by low-intensity IMES would include group I and II afferents and by painful IMES additionally group III afferents would be recruited (Laursen et al., 1999).

From an imaging point of view, somatosensory and pain studies have largely been concerned with brain processing of cutaneous or mixed afferent median nerve inputs. Both intracranial recordings and functional imaging studies have shown that a distributed network encompassing multiple cortical and subcortical areas processes somatosensory as well as nociceptive inputs. In a previous study of ours which used event-related functional magnetic resonance imaging (fMRI) to compare nonpainful and painful IMES (Niddam et al., 2002), nonpainful IMES was found to activate a subset of structures involved in painful IMES processing. The study also found motor-related activity in regions such as basal ganglia, primary motor cortex, lateral premotor area, as well as supplementary and cingulate motor areas. Further, based on the literature, a substantial overlap between central representations of acute muscle and cutaneous pain was demonstrated. However, it is well known that while fMRI provides good spatial resolution, it provides relatively little temporal information, because this methodology is based on hemodynamic mechanisms which do not directly reflect the neuronal response (Buckner, 1998; Rosen et al., 1998). In contrast to fMRI, electro- and magneto-encephalography (EEG/MEG) can provide information on a millisecond-by-millisecond basis. However, to date, only a few EEG studies have been concerned with IMES or muscle afferent (microstimulation) induced

* Corresponding author. Laboratory of Integrated Brain Research, Department of Medical Research and Education, Taipei Veterans General Hospital, No. 201, Sect. 2, Shih-Pai Road, Taipei 112, Taiwan. Fax: +886 2 28745182.
E-mail address: jchsieh@vghtpe.gov.tw (J.-C. Hsieh).
Available online on ScienceDirect (www.sciencedirect.com).

1053-8119/$ - see front matter © 2005 Elsevier Inc. All rights reserved.
doi:10.1016/j.neuroimage.2004.12.004

cortical activity, and these have dealt with characterizing peak waveforms or topographic patterns (Chen et al., 2000; Gandevia and Burke, 1990; Halonen et al., 1988; Kunesch et al., 1995; Niddam et al., 2001; Shimojo et al., 2000; Svensson et al., 1997). A single study used dipole modeling to assess activated brain regions (Shimojo et al., 2000). It concluded that the same areas were activated by skin and muscle stimulation. However, this study did not employ the procedures involved in high-resolution EEG mapping. Thus, no source imaging studies using IMES have been performed using high-resolution EEG or MEG.

The principal objective of the present study was, by means of high-resolution EEG, to assess the spatiotemporal scenario of brain activity associated with sensory stimulation of the abductor pollicis brevis muscle (APB) using IMES. Furthermore, the characteristics of this processing related to afferent nerve composition was investigated in a subpopulation of subjects by comparing the processing of muscle input to skin input. We reasoned that not only would the major difference in proprioceptive afferents be reflected in our data but, additionally, brain regions projecting to the muscles of the hand via direct spinal projections might also be involved, e.g., the cingulate motor area and lateral premotor cortex.

Materials and methods

Subjects

Eleven healthy right-handed male volunteers (mean age ± SD: 24.5 ± 2.2 years) participated in the study. Prior to the experiment, each subject gave informed consent to the experimental protocol, which had been approved by the Institutional Ethics Committee of Taipei Veterans General Hospital. The experiment was conducted in accordance with the Declaration of Helsinki. During the experiment subjects were seated in a comfortable reclining chair in a semi-darkened, electrically shielded room monitored by the experimenter.

Stimulation procedure

Intramuscular electrostimulation (square-wave, 1-ms duration, 1 Hz, Grass Telefactor S88 stimulator, W. Warwick, RI, USA) was delivered via a pair of needle electrodes (uninsulated tip, 20 mm long, 0.35-mm diameter, 2 mm^2 stimulation area, 1 cm separation; Model: 9013R0271 Medtronic Dantec, Denmark) inserted into the APB of the left hand. Additionally, in four subjects, the distal phalanx of the left thumb was stimulated (1-ms pulse; 1 Hz) with a pair of electrodes. One electrode was a conventional surface electrode placed at the tip of the thumb (anode, 9 mm × 6 mm; Model: 9013R0241 Medtronic Dantec, Denmark) and the other was a ring electrode (cathode) placed around the thumb distal to the interphalangeal joint. It is conceivably justified to compare stimulation of the thumb and the muscle since both sites are innervated by the median nerve. Furthermore, the skin surface above the thenar eminence and the thumb surface being stimulated belong to the same dermatome (C6). Stimulation of the digit is the easiest method to exclude muscle afferents from being activated by electrical stimulation and at the same time avoid muscular contraction which would confound our findings. In the IMES condition, two intensities were applied, nonpainful and painful, while in the surface condition, only a nonpainful intensity was used. Prior to SEP recordings, stimulus intensities were individually calibrated to correspond to the subjective rating of "intense but nonpainful" and "moderately painful" on an 11-point verbal descriptor scale (see Niddam et al., 2002). Stimulus intensity was reevaluated after each SEP recording session. Movement of the thumb was observed during stimulation at both intensities for IMES but not for surface stimulation of the thumb.

Data acquisition and preprocessing

A 64 electrode-montage (Quik-Cap, Neuromedical Supplies, USA) was used to record SEPs from the whole scalp. Electrodes were placed according to an augmented 10–20 system and included vertical and horizontal electrooculograms (bipolar recordings) in order to monitor eye movements. Before recordings, the three-dimensional location of all electrodes was obtained using a digitizer (Fastrack, Polhemus, USA), including the nasion and left and right preauricular points. All conditions were performed in separate sessions and repeated twice in a counterbalanced order across subjects. In total, SEP responses to 500 stimuli were registered per condition (linked-ears reference, scalp ground, sampling rate: 1 kHz, bandpass: 0.05–200 Hz, SynAmps, Neuroscan, Inc., USA). Epoch duration of SEPs ranged from 100 ms before to 750 ms after stimulus onset. Preprocessing (Scan 4.2, Neuroscan, Inc., USA) included baseline correction relative to the pre-stimulus interval, correction for linear trends and artifact rejection (criterion: ±60 μV; minimum 400 epochs were included). Before source analysis was performed, SEP data were transformed to a common average reference. Finally, after the SEP experiment, high-resolution magnetic resonance images (MRI; TR/TE/TI = 88.1 ms/4.12 ms/650 ms, 128 * 128 * 128 matrix, FOV = 192 mm) of the whole head were acquired on a 3.0-T Bruker MedSpec S300 system (Bruker, Kalsrube, Germany).

Dipole source reconstruction

Further steps involved in source modeling were performed using Curry software (Curry 4.6, Neuroscan, Inc., USA). Initially, digitized electrode positions were co-registered to anatomical landmarks on the individual MR image by matching nasion, left and right preauricular points obtained from digitization to those defined directly on the MR image. A realistic 3-layer (conductivities, scalp: 0.033 S/m, skull: 0.0042, and brain/liquor: 0.033 S/m) boundary element model (BEM) with about 4000 nodes, based on the individual MRI, was used for each subject (Fuchs et al., 2001). In addition, sources were constrained to a location within a compartment segmented from the gray matter of the individual cortex.

Data from each condition were explained by a multidipole model using a spatiotemporal approach. For each subject, global field power (GFP) was used to isolate stable topographical patterns (Lehmann and Skrandies, 1980). Based on these, the time course was divided into several subintervals of 10-ms duration in which the pattern was stable (for the two earliest dipoles in the surface stimulation condition, 5-ms intervals were used). Within each of these intervals, a single fixed equivalent current dipole was fitted to the measured data. In individuals with clear bitemporal activity, two dipoles were fitted simultaneously. In each time interval, the data were required to explain at least 80% of the data. Dipoles from all subintervals were combined in a model with time-varying source strengths but with fixed location and orientation to explain brain activity in the full time interval (−100 to 750 ms). Source location was reported according to a Talairach-based coordinate

system (Talairach and Tournoux, 1988) and dipole orientation given by the corresponding normal vectors (nx,ny,nz). In order to evaluate the *dislocation* of dipoles due to source location, source orientation, and noise in the signals, simulations of superficial tangential and deep radial sources were performed. One test-dipole was placed in the central sulcus and another one in the cingulate sulcus of a chosen subject (Subject 8). Two source strengths were used (10 and 20) and random zero-mean Gaussian noise was added to create comparable signal-to-noise ratios (SNR) to the mean SNR in the two IMES conditions (12 and 24, respectively). Dipole coordinates and orientations of the two sources were taken to approximate the grand mean values while maintaining the anatomical locations (Table 3). For the first source these were (x,y,z) = (35,−30, 44) and (nx,ny,nz) = (0.35,−0.87,−0.52), and for the second source, (x,y,z) = (7,−18, 43) and (nx,ny,nz) = (−0.03,−0.05, 0.85). Displacement error was defined as the square root of the sum of squares of the error in the 3 axes between the position of the original and fitted dipole. To obtain a reliable estimate of the error, the simulations were repeated 10 times for each parameter.

Statistics

Student's paired two-tailed t test was used to test for significant differences between the IMES conditions and between nonpainful IMES and surface conditions for stimulus current, subjective intensity rating (reported after SEP recordings) and SNR (relative to the baseline and excluding the stimulus artifact) of the SEPs. For consistent sources in the two IMES conditions (see below), the Wilcoxon test for paired data was used to test the following parameters: location (x,y,z), orientation (nx,ny,nz), peak dipole strength, peak latency, and onset/offset of activity. In all cases, a threshold value of $P < 0.05$ was required for results to be considered significant. Significant periods of activation for each dipole were extracted from the time interval which included the time point with maximal dipole strength and where the activity exceeded two standard deviations relative to the baseline (−100 to 0 ms). If a dipole did not fulfill these criteria in the final multi-dipole model, it was excluded and the model refitted.

Results

Stimulus intensity and ratings

The current applied during SEP recordings was 1.1 ± 0.3 mA, 3.0 ± 1.2 mA, and 4.7 ± 1.0 mA for nonpainful (NP) IMES, painful (P) IMES, and nonpainful surface stimulation of the skin (SURF), respectively. The stimulus current during NP IMES was significantly lower than both P IMES ($N = 11$; $P < 0.001$) and SURF ($N = 4$, $P < 0.001$). The subjective rating given after each SEP recording session was the same in the two nonpainful conditions (NP IMES: 2.5 ± 0.9; SURF: 2 ± 0.4) but significantly different between the two IMES conditions (P IMES: 5.7 ± 0.9; $P < 0.001$).

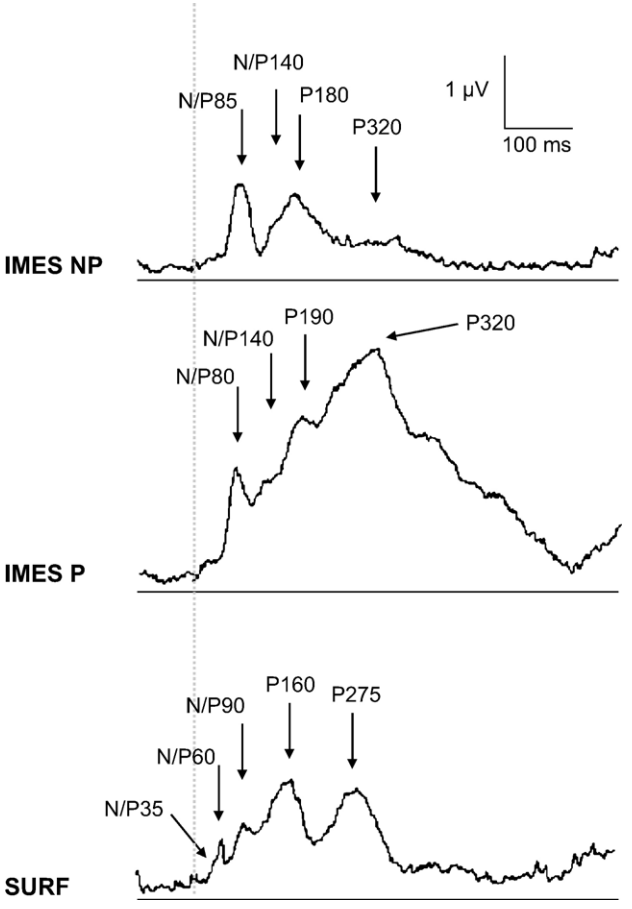

Fig. 1. GFP waveforms across 62 electrodes for Subject 8. Three conditions are shown: NP IMES (upper), P IMES (middle), and SURF (lower). Major peaks are marked according to the corresponding SEP peaks. The punctured vertical line through all plots denotes the stimulus onset (0 ms). The horizontal axis ranges from 100 ms before to 750 ms after stimulus onset.

SEP distribution

Painful IMES (SNR = 22.4 ± 8.6) resulted in a significantly larger SNR than nonpainful IMES ($N = 11$; $P = 0.015$). However, both nonpainful conditions showed comparable SNR values (N =

Table 1
Mean time window for dipole fits for nonpainful (NP) and painful (P) intramuscular electrical stimulation (IMES) and nonpainful electrical surface stimulation (SURF) of the thumb

	SMI	PM	cS2-Insula	iS2-Insula	ACC/CMA	PCC/PC
NP IMES	73.1–83.1 (7.0)	138.7–148.7 (26.0)	161.8–171.8 (38.8)	177.1–187.1 (55.2)	237.9–247.9 (29.7)	305.8–315.8 (51.2)
P IMES	68.9–78.9 (5.8)	120.6–130.6 (11.3)	168.4–178.4 (37.9)	151.8–161.8 (35.5)	245.8–255.8 (48.3)	318.5–328.5 (52.7)
SURF	39.3–44.3 (0.6)	–	108.3–118.3 (12.1)	118.0–128.0 (5.7)	176.0–186.0 (4.2)	245.8–255.8 (56.3)
	54.7–59.7 (1.5)					

Note. Start and end latencies of time windows are given in milliseconds. Standard deviations are given in parenthesis.
SMI: primary sensorimotor area; PM: premotor cortex; cS2/iS2-Insula: contralateral/ipsilateral operculo-insular cortices; CMA: cingulate motor area; ACC: anterior cingulate cortex; PCC/PC: posterior cingulate cortex/precuneus.

4; NP IMES: 14.75 ± 3.8; SURF: 13.8 ± 1.8). Based on the GFP, several time periods could be isolated with distinct topographies (Table 1). As an example, GFP peaks are shown in Fig. 1 for a single subject. Identifiable peaks in the two IMES conditions corresponded to (negative/positive-peak latency) N/P80–85, N/P140 (bilateral), P180–190, and P320. Although not visible in the GFP, the N/P140 pattern was persistently preceded by a distinct topographic pattern (N/P 125) in the nonpainful IMES condition and in half the subjects in the painful IMES condition. In the same subject (Fig. 1), the isolated peaks in response to skin stimulation were: N/P35, N/P60, N/P90 (bilateral), P160, and P275. An early N/P23 could be seen in the SEP waveforms but not in GFP. Overall, transitions between stable patterns appeared earlier in the skin than the two IMES conditions.

Source locations

Table 2 lists regions identified in individual source models. Contralaterally, these included SMI and lateral premotor area (PM). Medially, these included the anterior cingulate cortex (ACC), and an area involving the posterior cingulate cortex (PCC) and precuneus (PC). Bilaterally, the operculo-insular cortices (S2-Insula) were found to respond. In the SURF condition, two dipoles could be fitted in the SMI area at distinct time points. Other dipoles were located in SII-insula, ACC, and PCC/PC.

Table 2
Anatomical regions involved in SEP processing to nonpainful (NP) and painful (P) intramuscular electrical stimulation (IMES) and electrical surface stimulation (SURF)

	Ss	SMI	PM	S2-Insula	CMA/ACC	PCC/PC
NP IMES	1	+	+	+	+/–	–/+
	2	+	+	+	+/–	–
	3	+	+	–	+/–	+/–
	4	+	+	+	+/–	–/+
	5	+	+	++	–	+/–
	6	+	+	++	+/–	–
	7	+	+	–	+/–	+/–
	8	+	+	–	+/–	+/–
	9	+	+	–	+/–	+/–
	10	+	+	–	–	+/–
	11	+	+	–	+/–	–
P IMES	1	+	–	+	+/–	+/–
	2	+	+	+	+/–	–
	3	+	+	–	+/–	–/+
	4	+	–	++	+/–	–
	5	+	+	++	–	–/+
	6	+	–	++	+/–	–
	7	+	–	++	–	–/+
	8	+	–	++	+/–	–
	9	+	+	+	+/–	+/–
	10	+	+	+	+/–	–
	11					
NP SURF	8	++	–	++	–/+	+/–
	9	++	–	++	–/+	+/–
	10	++	–	+	–	+/–
	11	++	–	+	–	+/–

Note. Ss: subject; '+': a dipole, '++': two dipoles; '+++': three dipoles; '–': no dipole present. In the SII-Insula region, '+' denotes contralateral activity and '++' bilateral activity. Dipole analysis in Subject 11 was not performed for P IMES due to a bad SNR value (below 8).

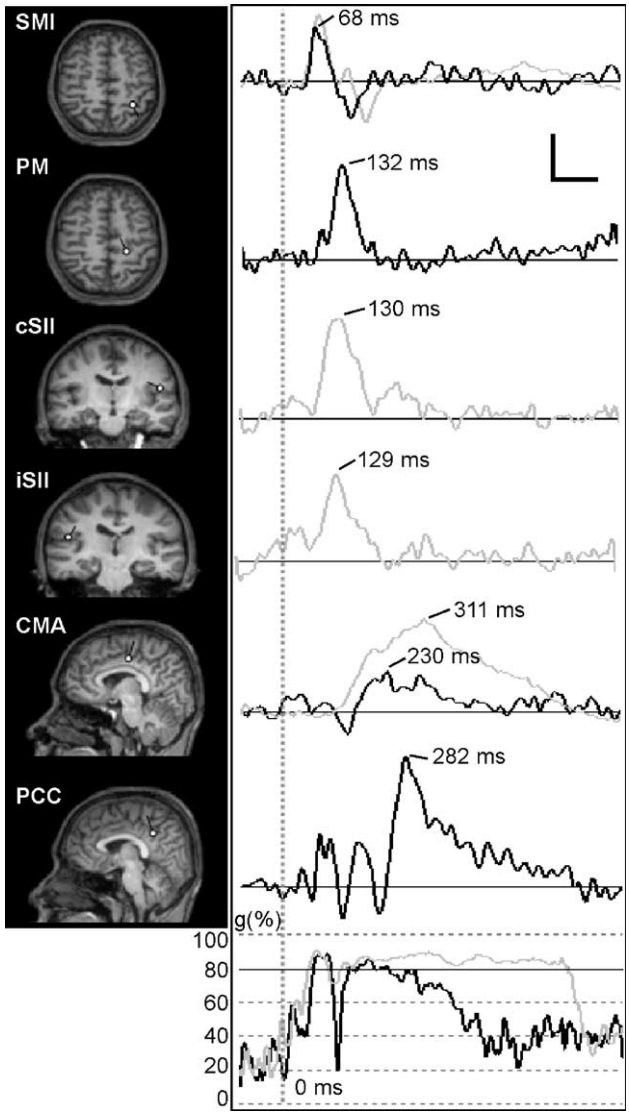

Fig. 2. Spatiotemporal source model (Subject 8) consisting of 4 sources for NP IMES and P IMES. Dipole locations are superimposed on individual MRI. Left: Source locations in SMI, lateral PM, contralateral and ipsilateral SII, caudal CMA and PCC are indicated with white dots. Common dipoles in the two IMES conditions are shown with the location for the NP IMES dipole. Black poles indicate the orientation of dipole sources. Left side of the images corresponds to the left hemisphere of the subject. Right: Time course of source strengths for the corresponding sources at left side are shown for NP IMES (black) and P IMES (gray). Peak strengths are marked together with their latencies. Time course of goodness of fit (g) for the multidipole model is shown at lower left side. The vertical calibration bar denotes 20 nAm for all source amplitudes except CMA where it denotes 40 nAm. The horizontal calibration bar denotes 100 ms.

Primary sensorimotor area (SMI)

The initial SMI dipoles to IMES were located within the wall of the central sulcus (Fig. 2, Table 3) for the majority of subjects. Location and orientation (tangential) were highly consistent between the two IMES conditions (N = 10; no significance). P IMES resulted in significantly stronger peak activation than NP IMES (N = 10; P = 0.028). However, timing (peak, onset and offset; N = 10) of the two sources was the same with peak activation around 75–85 ms after stimulation, corresponding to

Table 3
Source parameters in the multidipole model for responses to nonpainful and painful IMES

Source	Nonpainful IMES							Painful IMES					
	Location [mm]	Orientation	*q* max [μAmm]	Latency [ms]			GOF	Location [mm]	Orientation	*q* max [μAmm]	Latency [ms]			GOF
				Peak	Start	End					Peak	Start	End	
SMI	(36.5,−30.7, 46.1)	(0.32,−0.71,−0,47)	22*	80.1	41	101.5	96	(33.5,−32.7,45.6)	(0.36, −0.69, −0.45)	32.8*	75	46.1	110.4	96.2
	(7.1,8.0, 4.9)	(0.27,0.21,0.28)	8.9	10.7	12.1	11.5	2.5	(5.8,9.9,7.2)	(0.31,0.24,0.26)	10.2	9.9	7.2	17.9	3.3
PM	(29.7,−13.3,45.0)	(−0.37,0.19,0.25)	27.2	147.5	107.5	192.1	94.5	(32.7,−10.3,48.6)	(−0.86,0.30,0.0)	28.9	125.2	97	167.4	92.4
	(7.3,11.7,5.3)	(0.47,0.57,0.55)	15	33.3	25.9	45.5	3.8	(8.3,12.1,6.8)	(0.10,0.24,0.38)	10.3	22.8	22.9	36.1	6.1
S2-Insula (contralateral)	(37.6,−14.9,18.8)	(−0.60,0.03, −0.06)	17.9*	166.4	133.2	232.8	93.3	(36.2,−14.7,21.8)	(−0.45,−0.12,0.28)	34.7*	176.7	120	276.9	93.1
	(8.3,10.1,6.3)	(0.60,0.62,0.21)	9.8	39.5	33.1	70.9	2.1	(4.5,9.1,6.0)	(0.41,0.68,0.40)	12.2	48.9	43.6	95	3.8
S2-Insula (ipsilateral)	(−40.3,−18.7,18.2)	(0.86,0.26,0.11)	18.5	188	140.5	301	93.3	(−35.4,−20.8,22.7)	(0.66,0.46,0.41)	22.2	156.3	102	268	93.1
	(11.0,12.9,1.2)	(0.03,0.30,0.52)	4.1	55.2	18.7	125.9	2.1	(4.5,11.9,4.3)	(0.23,0.41,0.14)	12.6	46.3	26.9	99	3.8
CMA	(6.6,−18.3,43.2)	(−0.03,−0.05,0.85)	25.8*	242.3	192.8	379.5	93.4	(5.2,−14.6,43.0)	(−0.03,−0.25,0.91)	52.1*	249.1	174.7	390.6	93.7
	(11.1,7.0,5.4)	(0.17,0.50,0.20)	9.9	36.3	32.4	151	4.0	(11.2,7.2,3.8)	(0.27,0.18,0.07)	22.3	49	23.2	165.7	4.6
PCC/PC	(1.9,−39.2,33.8)	(0.11,0.04,0.54)	21.4*	310.8	259.4	425.4	90.3	(4.1,−39.2,43.9)	(−0.03,0.05,0.93)	43.9*	321.8	213.4	445.6	96.1
	(5.7,9.7,9.8)	(0.18,0.71,0.5)	10.3	97.9	106	158.8	5.6	(3.8,5.5,10.0)	(0.2,0.36,0.04)	18.5	96	76.7	152	1.8

Note. For each source, the first row gives the mean values and the second row gives the standard deviations. Coordinates (x,y,z) are given in a Talairach-based coordinate system defined relative to the individual anterior (AC) and posterior (PC) commissure with the origin at AC. The x-coordinate denotes the medial–lateral direction from the midline (+right,−left), the y-coordinate denotes the anteroposterior direction (+anterior,−posterior), and the z-coordinate denotes superior–inferior direction (+above,−below the line joining AC and PC). '*q* max': Maximum dipole strength. GOF: peak goodness of fit in intervals given in Table 1. Statistics was only performed on subjects showing dipole activation in both IMES conditions. See Table 1 for nomenclature.

* Significant difference between painful and nonpainful IMES.

simultaneous peaks in GFP. In the SURF condition, two SMI dipoles could be fitted. Both were located in the vicinity of the central sulcus but had slightly different orientation. In the GFP, the dipoles corresponded to N/P35 (shoulder) and N/P60. No dipole could be fitted to the earliest topographic pattern around 23 ms in any of the subjects, possibly due to too low SNR.

Lateral premotor cortex (PM)

Lateral premotor activity was seen in all subjects in response to NP IMES (Table 2) but in only half the subjects for P IMES. No PM source was found after surface stimulation. Apart from a single subject, the PM source was located in the middle and superior part of the precentral sulcus (Fig. 2). None of the parameters tested resulted in any differences. Note the corresponding GFP activity was embedded in the N/P140 peak (Fig. 1).

Operculo-insular cortices (S2-Insula)

Source location varied between subjects and covered the operculo-insular cortices encompassing the anterior–posterior insula and frontal–parietal operculum, including the secondary somatosensory area (Fig. 2). The S2-Insula sources were evident in GFP as N/P140 (Fig. 1). Opposite the preceding PM source, a larger number of subjects showed activity in S2-Insula when the IMES intensity was increased from nonpainful to painful (Table 2). Only contralateral peak source strength varied significantly between the two IMES conditions (Table 3; $N = 5$, $P = 0.008$), with the strongest response observed at painful intensity. Due to the insufficient number of subjects, no further statistical analysis was performed on the ipsilateral S2-Insula source parameters. In the SURF condition (N/P90 in Fig. 1), a contralateral response was evident in all subjects.

Anterior cingulate cortex (ACC)/cingulate motor area (CMA)

In the IMES conditions, the dipole source (corresponding to P180–190 in Fig. 1) was located contralaterally around both the upper and lower bank of the cingulate sulcus and slightly posterior to the vertical line through the AC point (VAC; Fig. 2, Table 3). This location agrees with the suggested hand representation of caudal CMA (Paus, 2001; Vogt and Vogt, 2003). Of the dipole parameters, only peak source strength changed significantly (Table 3; $N = 7$, $P = 0.026$) with P IMES resulting in strongest peak activity. The CMA source also satisfactorily explained the latest GFP peak (P320 in Fig. 1) in several of the subjects. However, this occurred mostly for P IMES. In the SURF condition (P160 in Fig. 1), the source was located in the caudal part of the anterior cingulate gyrus.

Posterior medial region (PCC/PC)

Location varied from the posterior cingulate cortex (PCC), covering Brodmann area 23 or 31, to the precuneus (PC), and was posterior to the vertical line through the PC point in all subjects (Fig. 2, Table 3). The only significant difference in dipole parameters was found for peak strength with P IMES resulting in strongest activity ($N = 5$; $P = 0.032$). In GFP (Fig. 1), the PCC/PC activity was seen as a major peak corresponding to P320 and P275 for IMES and SURF, respectively (see Table 4).

Simulations

For the best fit to the test-dipole located in the central sulcus, the displacement relative to the original source location was on

Table 4
Source parameters in the multidipole model for responses to nonpainful surface stimulation (SURF)

Source	Location [mm]	Orientation	q max [μAmm]	Latency [ms]			GOF
				Peak	Start	End	
SMI							
Dipole 1	(33.8,−28.7,49.2)	(0.57,−0.69,0.06)	8.6	42	33.3	54.3	96.1
	(11.3,4.1,6.5)	(0.26,0.27,0.37)	2.5	1	1.2	5.7	2.5
Dipole 2	(34.3,−32.0,50.6)	(0.46,−0.61,0.44)	11.2	59	50.3	70.7	96.1
	(3.7, 9.5, 8.9)	(0.10,0.19,0.53)	3.5	3	11.1	3.8	1.3
S2-Insula (contralateral)	(37.4,−16.5,20.4)	(−0.67,0.13,−0.12)	22.6	109.5	79.5	151.8	94.8
	(5.1,11.4,5.1)	(0.29,0.53,0.57)	18.3	13.3	13.5	5.9	2.6
S2-Insula (ipsilateral)	(−34.3,−26.0,22.4)	(0.77,0.34,0.05)	19.9	118.5	93.5	152.5	94.8
	(8.8,4.2,5.3)	(0.28,0.60,0.38)	7.3	27.6	31.8	3.5	2.6
ACC	(8.5,−20.0,35.4)	(0.33,−0.43,0.84)	41.9	177	145.5	283.5	96.4
	(4.4,9.2,4.0)	(0,0.13,0.06)	5.8	1.4	3.5	111	0.2
PCC	(11.4,−38.3,38.5)	(0.13,0.25,0.92)	24.9	248.5	179	334.8	96.1
	(5.0,4.9,5.7)	(0.2,0.23,0.10)	6.6	59	63.7	86.7	1.2

See Table 1 for nomenclature and Table 3 for further description.

average 3.0 mm for the low SNR and 1.5 mm for the high SNR. For the best fit to the test-dipole located in the cingulate sulcus, the values were 3.1 mm and 1.2 mm, respectively. It should be born in mind that these values do not take digitization errors of the electrode position into account as well as co-registration errors of the MRI and electrode positions and errors in BEM.

Discussion

This study used high-resolution EEG to elucidate the spatio-temporal brain processing to IMES. The chosen strategy of fitting dipole sources independently for each IMES condition resulted in consistent locations across subjects. The same sources were involved in both NP and P IMES supporting the notion that NP IMES activates a subset of structures involved in P IMES (Niddam et al., 2002). Source locations found in the present study agrees with activations listed in a previous event-related fMRI study of ours (Niddam et al., 2002). As expected, the brain structures involved in IMES processing are related to both primary and higher order sensory and motor processing.

The responding brain areas to electrostimulation of the digit in the present study largely agreed with the most commonly observed sources from the literature. Sources have been localized in primary sensory area (SI), bilateral SII, and the medial wall corresponding to either supplementary motor area (SMA) or mid cingulate gyrus (Buchner et al., 1994; Dowman and Schell, 1999; Kitamura et al., 1995; Ninomiya et al., 2001; Yamasaki et al., 2000). However, it is well known that within the first 50-ms poststimulus, a complex activation pattern can be observed in vicinity of SI. A recent SEF study stimulating the dorsum of the hand showed a clear serial temporal organization of somatosensory processing including areas 3b, 4 and 1, and PPC (Inui et al., 2004).

A larger body of literature exists for SEPs/SEFs to MN stimulation at the wrist than digit stimulation. Although contralateral SI and bilateral SII sources have been shown to be sufficient to model SEF data (Lin et al., 2003), an additional source has been located in contralateral PPC for both SEPs and SEFs (Forss et al., 1994; Mauguiere et al., 1997a; Valeriani et al., 2000). Other sources have been localized in cingulate gyrus, PC, and PM area (Mauguiere et al., 1997a; Waberski et al., 2002).

Characteristics of IMES processing

The source configuration found for IMES processing in the present study exhibit pronounced differences from the source model obtained after skin stimulation. First, in the early post-stimulus phase, the first SEP component to IMES peaked after 75–85 ms and the corresponding SMI source had an onset around 40 ms and could be explained by a single dipole. For SURF, several SEP components were found within the first 60 ms after stimulus onset and the source onset was around 33 ms (not including the N/P23 response). Furthermore, two dipoles had to be included in order to account for the data. This finding has consistently been observed in our group for SEPs (Niddam et al., 2001) as well as for SEFs (unpublished data) to IMES. Second, a lateral premotor source was found to follow the initial SMI source activity after IMES but in none of the subjects after SURF. Third, rather than being located in the cingulate gyrus, the first medial source was consistently located in the cingulate sulcus corresponding to caudal CMA (Paus, 2001; Vogt and Vogt, 2003). The significance of these issues will be discussed further below.

Primary sensorimotor area

Considering afferent projection to SMI in the context of muscle stimulation, it is appropriate to compare SEPs to both *digit and MN stimulation* as well as proprioceptive induced activity by *passive movement*. The initial SEP pattern to *IMES* was bipolar and peaked 80–90 ms poststimulus. The corresponding source was located deep in the wall of the central sulcus and could either be in the hand representation of area 3b of SI or area 4 of primary motor cortex (MI).

Several of the early SEP components observed within 60 ms after stimulus onset for *digit and MN stimulation* have been localized to area 3b and area 1 of primary somatosensory cortex (SI) (Allison et al., 1989a,b; Buchner et al., 1994) and are mainly dominated by cutaneous inputs (Allison et al., 1991; Halonen et al., 1988; Kunesch et al., 1995). This is in agreement with both area 3b and area 1 being main targets for projections from cutaneous Aβ-fiber afferents (Mima et al., 1997).

Proprioceptive evoked activity is processed in areas 3a and 2 of SI. Further, both area 3b and area 4 (MI) receive inputs from area 3a (Fetz et al., 1980; Heath et al., 1976; Huerta and Pons, 1990;

Mima et al., 1997). In SEPs to passive movement, a bipolar pattern around 80–90 ms postmovement can be observed (N/P90; Alary et al., 1998; Seiss et al., 2002) and in the corresponding SEFs, earlier field deflections have been observed with possible origin in area 3a (P1 deflection) and the following deflections with possible origin in area 3b and/or area 4 (P2 and P3; Alary et al., 2002; Druschky et al., 2003; Xiang et al., 1997). The early deflection in SEFs might not be visible in the present SEP data due to too low SNR. The N/P90 pattern in SEPs is thought to be dominated by muscle spindle input and the generator of this pattern has, contentiously, been located anterior to that of N/P23 (area 3b) in area 4 (Seiss et al., 2002, 2003).

Overall, N/P80–85 to IMES, N/P60 to MN, and digit stimulation and N/P90 to passive movement all consist of approximately the same bipolar pattern with the same polarity. In the present study, no systematic intraindividual difference in location was noted between N/P60 to digit stimulation and N/P80–85 to IMES. Nonetheless, two factors point to a proprioceptive origin either from area 3b or area 4 via area 3a. Firstly, a substantially longer latency was found for IMES than digit stimulation. Both latency and the corresponding topographical distribution match the one observed after passive movement. Secondly, in several subjects, a shoulder on the rising phase of the frontocentral negative peak was observed around 60 ms, and in a few subjects at low IMES intensity, a dissociation of the N60 and N80–85 peaks was observed. These two peaks might correspond to the P2 and P3 field deflections in Xiang et al. (1997). Although it remains speculative to assign specific anatomical subregions to the SMI source, it is tempting to suggest that the N/P60-shoulder and the N/P80–85 peaks to IMES are generated by proprioceptive input in area 3b and area 4, respectively.

Lateral premotor area

The present study revealed a consistent activation of the dorso-lateral premotor area to nonpainful IMES. Somatosensory-induced activity in PM area has only rarely been described in relation to SEP/SEFs. In two cases, MN was stimulated and the source was located anterior to the precentral sulcus in vicinity of middle frontal gyrus (Mauguiere et al., 1997a,b; Waberski et al., 2002). Mauguiere et al. (1997a,b) found the source to peak around 129 ms poststimulus with a latency range of 100–170 ms and with a substantial interindividual scatter in location. Both studies suggested a mesial origin. Since the source presented here is located in vicinity of precentral sulcus on the dorso-lateral surface, it is unclear whether the reported sources represent the same functional area. A possible explanation for the reduced occurrence of the dorso-lateral PM source in response to painful IMES is that it was masked by the coincident and larger activity in contralateral operculo-insular cortices. It is well known that activity in this region highly depends on the stimulus intensity, especially at painful levels (Torquati et al., 2002). In agreement with this, the present results showed a more consistent operculo-insular activity in the painful condition as well as a stronger dipole moment.

In recent years, profound changes have taken place in the view of how medial and lateral PM areas are organized. Largely, this insight has come about through study of nonhuman primates (for reviews, see Dum and Strick, 2002; Hoshi and Tanji, 2004; Paus, 2001; Rizzolatti and Luppino, 2001; Rizzolatti et al., 1998; Tanji, 1996) but increasingly also through neuroimaging studies of humans (Gelnar et al., 1999; Koski and Paus, 2000; Kwan et al., 2000; Paus et al., 1998; Picard and Strick, 2001). Overall, both medial and lateral regions can be divided according to their main connectivity to either prefrontal cortex or to MI and spinal cord. Where areas with direct connection to MI and direct corticospinal projections are involved in sensory–motor transformations through a fronto-parietal network, areas with prefrontal connections promise the possibility of cognitive control over motor output. The superior part of precentral sulcus has been proposed to be homologue to dorso-lateral area F2 in monkeys (Rizzolatti et al., 1998). It is interconnected to other PM areas, has reciprocal connections with parietal sensory areas, projects directly to MI and spinal motor neurons, and contains a representation of the arm (Raos et al., 2003). Evidence suggests the region to be involved in planning, preparation, and control of movement based on sensory information from parietal areas. Preliminary results have indicated the area to respond to proprioceptive stimuli (Rizzolatti et al., 1998). Since subjects in the present study did not perform any voluntary movement, the source activity in lateral PM might represent integration of somatosensory feedback from the muscle for shaping of potential motor actions.

Caudal cingulate motor area

Both nonpainful and painful IMES resulted in a dipole source located around contralateral dorsal and ventral banks of cingulate sulcus slightly posterior to VAC in agreement with the location of caudal CMA (Vogt and Vogt, 2003). It is well known that anterior cingulate cortex is a heterogeneous structure which can be further subdivided according to cytoarchitectonics, connectivity, and function. Within both human and nonhuman primate ACC, multiple CMAs have been suggested to exist (Dum and Strick, 1992; Fink et al., 1997; Matelli et al., 1991; Paus, 2001; Picard and Strick, 2001; Vogt and Vogt, 2003). Currently, subdivisions of CMAs in nonhuman primates have been done in two partially overlapping ways resulting in a conflicting concept of somatotopy (Dum and Strick, 1992; Luppino et al., 1991; Matelli et al., 1991). In humans, a rostral and a caudal CMA have been proposed to exist. A recent cytological study in humans (Vogt and Vogt, 2003) found evidence for further subdivision of caudal CMA with distinct areas at dorsal and ventral banks of cingulate sulcus. Both dorsal and ventral areas were localized along the sulcal region between VAC and approximately 2 cm posterior to this plane (Vogt and Vogt, 2003).

Human caudal CMA is activated during motor paradigms (Fink et al., 1997; Paus, 2001; Picard and Strick, 2001) and has been suggested, based on responses to finger movement, to contain a hand area (Kwan et al., 2000; Paus, 2001; Paus et al., 1998; Picard and Strick, 2001). It is a distinct locus that can be functionally segregated from the surrounding SMA proper as well as from pain-specific area of ACC (Kwan et al., 2000). In humans, effective connectivity has been found between CMAs and both MI and SMA (Koski and Paus, 2000) in agreement with results from nonhuman primates showing reciprocal connections (Luppino et al., 1993; Morecraft and Van Hoesen, 1992). Other regions known to be targets for projections from nonhuman caudal CMA include dorso-lateral PM area (F2), posterior medial regions in parietal as well as cingulate cortex, insula, and orbitofrontal cortex (Luppino et al., 2003; Mesulam and Mufson, 1982; Morecraft and Van

Hoesen, 1998; Vogt and Pandya, 1987). Finally, caudal CMA has direct corticospinal projections terminating on spinal motorneurons innervating the muscles of the fingers and wrist (Biber et al., 1978; Dum and Strick, 1991, 1996; He et al., 1995; Strick et al., 1998). Based on this network, it has been suggested that CMAs are involved in direct control of skeletomotor function and constitutes the pivotal point of limbic influence over voluntary motor system (Morecraft and Van Hoesen, 1998). Since neuronal responses precede movement onset (Shima et al., 1991), such influence is likely exerted in the planning and preparatory phase of movement and is based on sensory stimuli as well as cognitive interaction. In context of the present results, the CMA response might reflect the integrated somatosensory and cognitive substrate upon which control and/or selection of motor responses from planned motor actions is based.

Temporal cascade of activity

In terms of timing and propagation of IMES SEP source activity, a segregation into parallel sensory–discriminative and sensory–motor streams likely occurs. As previously mentioned, it is well known that proprioceptive inputs are processed in both SI and MI for which close interconnections exist. From all subdivisions of SI, direct projections exist for somatosensory and nociceptive inputs to SII (Friedman et al., 1986), and from MI projections exist to dorso-lateral PM area as well as caudal CMA and between the two premotor areas (Luppino et al., 2003). Apparently, no direct connections exist between SII and the two premotor areas (Friedman et al., 1986). However, inputs from SII might reach caudal CMA via insula (Friedman et al., 1986; Mesulam and Mufson, 1982; Vogt and Pandya, 1987). As mentioned above, connections exist from caudal CMA to the posterior medial wall containing both precuneus and posterior cingulate cortex (Morecraft and Van Hoesen, 1998; Vogt and Pandya, 1987). Thus, the suggested parallel processing revealed here might on one hand subserve higher order sensory processing related to sensory discrimination via SI and SII and on the other hand integration of sensory feedback from the muscle possibly related to generation and selection of plans for further motor processing via MI, PM area, and caudal CMA.

Latency differences

In agreement with a previous study, longer latencies were generally found after IMES than cutaneous stimulation (Shimojo et al., 2000). Longer latencies have also been found for passive movement compared to cutaneous stimulation in SEFs (Druschky et al., 2003; Xiang et al., 1997). A likely explanation of this discrepancy could be the different pathways of processing as indicated by the present study. As previously mentioned, the early N/P80–85 response most likely does not reflect the primary component in SI but rather a secondary component in either area 3b or area 4. Also, muscle inputs are possibly relayed from SMI either directly via dorso-lateral PM or additionally via the parietal higher order sensory areas before they arrive at CMA and PCC (Luppino et al., 2003; Rizzolatti and Luppino, 2001). An additional plausible explanation is that the often diffuse sensation evoked by IMES or passive movement is less successful in time locking SEP responses and therefore creates latency jitter. This could partially also explain the large interindividual variation observed in SEFs to passive movement.

Commentary on method

To augment the anatomical allocations in the present study based on the spatial resolution of the given method, we evaluated the influence of dipole location, dipole orientation, and noise on localization accuracy through dipole simulations. In agreement with Whittingstall et al. (2003), the simulations showed the same error margin was introduced by noise at both superficial and deep sources with the high SNR resulting in the smallest error (app. 1.5 mm and 3 mm). This has previously been found to be the case for SNRs above a certain threshold (Whittingstall et al., 2003). Such an error should be seen in light of the location error due to the use of BEMs which has been estimated to be around 7–8 mm (Leahy et al., 1998). Within these error bounds, the interpretation of our results is reasonable in the context of the given resolution.

Conclusions

Complementing our previous findings using event-related fMRI (Niddam et al., 2002), the temporal evolution of brain activity to nonpainful and painful IMES was mapped. The present study demonstrated a characteristic pattern of brain processing related to muscle sensory inputs evoked by IMES compared to the processing from cutaneous sensory inputs evoked by electro-stimulation of the digit. Based on the involvement of both sensory and motor areas, we suggest muscle sensory inputs can be processed in two parallel streams subserving higher order sensory processing as well as sensory–motor integration. One stream likely involves sensory discrimination while the other involves integration of sensory feedback on which further motor processing is based. Finally, this study demonstrated that a well-characterized brief stimulus can evoke reproducible responses from premotor areas related to muscle sensory afferents. These findings provide basis for further insight to central effects of muscle-related pathological pain such as, e.g., myofascial pain syndrome or fibromyalgia where altered peripheral nerve transmission exist and supraspinal factors might be important for the understanding of hypersensitivity (Gracely et al., 2002).

Acknowledgments

This study was funded by National Science Council (932314B075084, 922314B075095, 912314B075069, 912314B075069, 902314B075115, 902314B075124, 902314B075115), National Health and Research Institute (EX93-9332SI), and Taipei Veterans General Hospital (933561, 93322) of Taiwan. Special thanks to Mr. Chi-Cher Chou for MRI technical assistance and Miss Ching-Sui Hung, Mr. Cheng-Hao Tu and Mr. Chin-Hung Lin for assistance with practical issues during the experiment.

References

Abrahams, V.C., 1986. Group III and IV receptors of skeletal muscle. Can. J. Physiol. Pharmacol. 64, 509–514.

Alary, F., Doyon, B., Loubinoux, I., Carel, C., Boulanouar, K., Ranjeva, J.P., Celsis, P., Chollet, F., 1998. Event-related potentials elicited by passive movements in humans: characterization, source analysis, and comparison to fMRI. NeuroImage 8, 377–390.

Alary, F., Simoes, C., Jousmaki, V., Forss, N., Hari, R., 2002. Cortical activation associated with passive movements of the human index finger: an MEG study. NeuroImage 15, 691–696.

Allison, T., McCarthy, G., Wood, C.C., Darcey, T.M., Spencer, D.D., Williamson, P.D., 1989a. Human cortical potentials evoked by stimulation of the median nerve. II. Cytoarchitectonic areas generating short-latency activity. J. Neurophysiol. 62, 694–710.

Allison, T., McCarthy, G., Wood, C.C., Williamson, P.D., Spencer, D.D., 1989b. Human cortical potentials evoked by stimulation of the median nerve. II. Cytoarchitectonic areas generating long-latency activity. J. Neurophysiol. 62, 711–722.

Allison, T., McCarthy, G., Wood, C.C., Jones, S.J., 1991. Potentials evoked in human and monkey cerebral cortex by stimulation of the median nerve. A review of scalp and intracranial recordings. Brain 114, 2465–2503.

Biber, M.P., Kneisley, L.W., LaVail, J.H., 1978. Cortical neurons projecting to the cervical and lumbar enlargements of the spinal cord in young and adult rhesus monkeys. Exp. Neurol. 59, 492–508.

Buchner, H., Fuchs, M., Wischmann, H.A., Dossel, O., Ludwig, I., Knepper, A., Berg, P., 1994. Source analysis of median nerve and finger stimulated somatosensory evoked potentials: multichannel simultaneous recording of electric and magnetic fields combined with 3D-MR tomography. Brain Topogr. 6, 299–310.

Buckner, R.L., 1998. Event-related fMRI and the hemodynamic response. Hum. Brain Mapp. 6, 373–377.

Chen, A.C., Shimojo, M., Svensson, P., Arendt-Nielsen, L., 2000. Brain dynamics of scalp evoked potentials and current source densities to repetitive (5-pulse train) painful stimulation of skin and muscle: central correlate of temporal summation. Brain Topogr. 13, 59–72.

Dowman, R., Schell, S., 1999. Innocuous-related sural nerve-evoked and finger-evoked potentials generated in the primary somatosensory and supplementary motor cortices. Clin. Neurophysiol. 110, 2104–2116.

Druschky, K., Kaltenhauser, M., Hummel, C., Druschky, A., Huk, W.J., Neundorfer, B., Stefan, H., 2003. Somatosensory evoked magnetic fields following passive movement compared with tactile stimulation of the index finger. Exp. Brain Res. 148, 186–195 (Electronic publication 2002 Nov 20).

Dum, R.P., Strick, P.L., 1991. The origin of corticospinal projections from the premotor areas in the frontal lobe. J. Neurosci. 11, 667–689.

Dum, R.P., Strick, P.L., 1992. Medial wall motor areas and skeletomotor control. Curr. Opin. Neurobiol. 2, 836–839.

Dum, R.P., Strick, P.L., 1996. Spinal cord terminations of the medial wall motor areas in macaque monkeys. J. Neurosci. 16, 6513–6525.

Dum, R.P., Strick, P.L., 2002. Motor areas in the frontal lobe of the primate. Physiol. Behav. 77, 677–682.

Fetz, E.E., Finocchio, D.V., Baker, M.A., Soso, M.J., 1980. Sensory and motor responses of precentral cortex cells during comparable passive and active joint movements. J. Neurophysiol. 43, 1070–1089.

Fink, G.R., Frackowiak, R.S., Pietrzyk, U., Passingham, R.E., 1997. Multiple nonprimary motor areas in the human cortex. J. Neurophysiol. 77, 2164–2174.

Forss, N., Hari, R., Salmelin, R., Ahonen, A., Hamalainen, M., Kajola, M., Knuutila, J., Simola, J., 1994. Activation of the human posterior parietal cortex by median nerve stimulation. Exp. Brain Res. 99, 309–315.

Friedman, D.P., Murray, E.A., O'Neill, J.B., Mishkin, M., 1986. Cortical connections of the somatosensory fields of the lateral sulcus of macaques: evidence for a corticolimbic pathway for touch. J. Comp. Neurol. 252, 323–347.

Fuchs, M., Wagner, M., Kastner, J., 2001. Boundary element method volume conductor models for EEG source reconstruction. Clin. Neurophysiol. 112, 1400–1407.

Gandevia, S.C., Burke, D., 1990. Projection of thenar muscle afferents to frontal and parietal cortex of human subjects. Electroencephalogr. Clin. Neurophysiol. 77, 353–361.

Gelnar, P.A., Krauss, B.R., Sheehe, P.R., Szeverenyi, N.M., Apkarian, A.V., 1999. A comparative fMRI study of cortical representations for thermal painful, vibrotactile, and motor performance tasks. NeuroImage 10, 460–482.

Gracely, R.H., Petzke, F., Wolf, J.M., Clauw, D.J., 2002. Functional magnetic resonance imaging evidence of augmented pain processing in fibromyalgia. Arthritis Rheum. 46, 1333–1343.

Halonen, J.P., Jones, S., Shawkat, F., 1988. Contribution of cutaneous and muscle afferent fibres to cortical SEPs following median and radial nerve stimulation in man. Electroencephalogr. Clin. Neurophysiol. 71, 331–335.

He, S.Q., Dum, R.P., Strick, P.L., 1995. Topographic organization of corticospinal projections from the frontal lobe: motor areas on the medial surface of the hemisphere. J. Neurosci. 15, 3284–3306.

Heath, C.J., Hore, J., Phillips, C.G., 1976. Inputs from low threshold muscle and cutaneous afferents of hand and forearm to areas 3a and 3b of baboon's cerebral cortex. J. Physiol. 257, 199–227.

Hoshi, E., Tanji, J., 2004. Functional specialization in dorsal and ventral premotor areas. Prog. Brain Res. 143, 507–511.

Huerta, M.F., Pons, T.P., 1990. Primary motor cortex receives input from area 3a in macaques. Brain Res. 537, 367–371.

Inui, K., Wang, X., Tamura, Y., Kaneoke, Y., Kakigi, R., 2004. Serial processing in the human somatosensory system. Cereb. Cortex 14, 851–857 (Electronic publication 2004 Mar 28).

Kitamura, Y., Kakigi, R., Hoshiyama, M., Koyama, S., Shimojo, M., Watanabe, S., 1995. Pain-related somatosensory evoked magnetic fields. Electroencephalogr. Clin. Neurophysiol. 95, 463–474.

Koski, L., Paus, T., 2000. Functional connectivity of the anterior cingulate cortex within the human frontal lobe: a brain-mapping meta-analysis. Exp. Brain Res. 133, 55–65.

Kunesch, E., Knecht, S., Schnitzler, A., Tyercha, C., Schmitz, F., Freund, H.J., 1995. Somatosensory evoked potentials elicited by intraneural microstimulation of afferent nerve fibers. J Clin. Neurophysiol. 12, 476–487.

Kwan, C.L., Crawley, A.P., Mikulis, D.J., Davis, K.D., 2000. An fMRI study of the anterior cingulate cortex and surrounding medial wall activations evoked by noxious cutaneous heat and cold stimuli. Pain 85, 359–374.

Laursen, R.J., Graven-Nielsen, T., Jensen, T.S., Arendt-Nielsen, L., 1999. The effect of differential and complete nerve block on experimental muscle pain in humans. Muscle Nerve 22, 1564–1570.

Leahy, R.M., Mosher, J.C., Spencer, M.E., Huang, M.X., Lewine, J.D., 1998. A study of dipole localization accuracy for MEG and EEG using a human skull phantom. Electroencephalogr. Clin. Neurophysiol. 107, 159–173.

Lehmann, D., Skrandies, W., 1980. Reference-free identification of components of checkerboard-evoked multichannel potential fields. Electroencephalogr. Clin. Neurophysiol. 48, 609–621.

Lin, Y.Y., Shih, Y.H., Chen, J.T., Hsieh, J.C., Yeh, T.C., Liao, K.K., Kao, C.D., Lin, K.P., Wu, Z.A., Ho, L.T., 2003. Differential effects of stimulus intensity on peripheral and neuromagnetic cortical responses to median nerve stimulation. NeuroImage 20, 909–917.

Luppino, G., Matelli, M., Camarda, R.M., Gallese, V., Rizzolatti, G., 1991. Multiple representations of body movements in mesial area 6 and the adjacent cingulate cortex: an intracortical microstimulation study in the macaque monkey. J. Comp. Neurol. 311, 463–482.

Luppino, G., Matelli, M., Camarda, R., Rizzolatti, G., 1993. Corticocortical connections of area F3 (SMA-proper) and area F6 (pre-SMA) in the macaque monkey. J. Comp. Neurol. 338, 114–140.

Luppino, G., Rozzi, S., Calzavara, R., Matelli, M., 2003. Prefrontal and agranular cingulate projections to the dorsal premotor areas F2 and F7 in the macaque monkey. Eur J. Neurosci. 17, 559–578.

Matelli, M., Luppino, G., Rizzolatti, G., 1991. Architecture of superior and mesial area 6 and the adjacent cingulate cortex in the macaque monkey. J. Comp. Neurol. 311, 445–462.

Mauguiere, F., Merlet, I., Forss, N., Vanni, S., Jousmaki, V., Adeleine, P., Hari, R., 1997a. Activation of a distributed somatosensory cortical network in the human brain. A dipole modelling study of magnetic fields evoked by median nerve stimulation. Part I: Location and

activation timing of SEF sources. Electroencephalogr. Clin. Neurophysiol. 104, 281–289.
Mauguiere, F., Merlet, I., Forss, N., Vanni, S., Jousmaki, V., Adeleine, P., Hari, R., 1997b. Activation of a distributed somatosensory cortical network in the human brain: a dipole modelling study of magnetic fields evoked by median nerve stimulation. Part II: effects of stimulus rate, attention and stimulus detection. Electroencephalogr. Clin. Neurophysiol. 104, 290–295.
Mesulam, M.M., Mufson, E.J., 1982. Insula of the old world monkey. III: efferent cortical output and comments on function. J. Comp. Neurol. 212, 38–52.
Mima, T., Ikeda, A., Terada, K., Yazawa, S., Mikuni, N., Kunieda, T., Taki, W., Kimura, J., Shibasaki, H., 1997. Modality-specific organization for cutaneous and proprioceptive sense in human primary sensory cortex studied by chronic epicortical recording. Electroencephalogr. Clin. Neurophysiol. 104, 103–107.
Morecraft, R.J., Van Hoesen, G.W., 1992. Cingulate input to the primary and supplementary motor cortices in the rhesus monkey: evidence for somatotopy in areas 24c and 23c. J. Comp. Neurol. 322, 471–489.
Morecraft, R.J., Van Hoesen, G.W., 1998. Convergence of limbic input to the cingulate motor cortex in the rhesus monkey. Brain Res. Bull. 45, 209–232.
Niddam, D.M., Graven-Nielsen, T., Arendt-Nielsen, L., Chen, A.C., 2001. Non-painful and painful surface and intramuscular electrical stimulation at the thenar and hypothenar sites: differential cerebral dynamics of early to late latency SEPs. Brain Topogr. 13, 283–292.
Niddam, D.M., Yeh, T.C., Wu, Y.T., Lee, P.L., Ho, L.T., Arendt-Nielsen, L., Chen, A.C., Hsieh, J.C., 2002. Event-related functional MRI study on central representation of acute muscle pain induced by electrical stimulation. NeuroImage 17, 1437–1450.
Ninomiya, Y., Kitamura, Y., Yamamoto, S., Okamoto, M., Oka, H., Yamada, N., Kuroda, S., 2001. Analysis of pain-related somatosensory evoked magnetic fields using the MUSIC (multiple signal classification) algorithm for magnetoencephalography. NeuroReport 12, 1657–1661.
Paus, T., 2001. Primate anterior cingulate cortex: where motor control, drive and cognition interface. Nat. Rev., Neurosci. 2, 417–424.
Paus, T., Koski, L., Caramanos, Z., Westbury, C., 1998. Regional differences in the effects of task difficulty and motor output on blood flow response in the human anterior cingulate cortex: a review of 107 PET activation studies. NeuroReport 9, R37–R47.
Picard, N., Strick, P.L., 2001. Imaging the premotor areas. Curr. Opin. Neurobiol. 11, 663–672.
Raos, V., Franchi, G., Gallese, V., Fogassi, L., 2003. Somatotopic organization of the lateral part of area F2 (dorsal premotor cortex) of the macaque monkey. J. Neurophysiol. 89, 1503–1518.
Rizzolatti, G., Luppino, G., 2001. The cortical motor system. Neuron 31, 889–901.
Rizzolatti, G., Luppino, G., Matelli, M., 1998. The organization of the cortical motor system: new concepts. Electroencephalogr. Clin. Neurophysiol. 106, 283–296.
Rosen, B.R., Buckner, R.L., Dale, A.M., 1998. Event-related functional MRI: past, present, and future. Proc. Natl. Acad. Sci. U. S. A. 95, 773–780.
Seiss, E., Hesse, C.W., Drane, S., Oostenveld, R., Wing, A.M., Praamstra, P., 2002. Proprioception-related evoked potentials: origin and sensitivity to movement parameters. NeuroImage 17, 461–468.
Seiss, E., Praamstra, P., Hesse, C.W., Rickards, H., 2003. Proprioceptive sensory function in Parkinson's disease and Huntington's disease: evidence from proprioception-related EEG potentials. Exp. Brain Res. 148, 308–319 (Electronic publication 2002 Nov 30.).
Shima, K., Aya, K., Mushiake, H., Inase, M., Aizawa, H., Tanji, J., 1991. Two movement-related foci in the primate cingulate cortex observed in signal-triggered and self-paced forelimb movements. J. Neurophysiol. 65, 188–202.
Shimojo, M., Svensson, P., Arendt-Nielsen, L., Chen, A.C., 2000. Dynamic brain topography of somatosensory evoked potentials and equivalent dipoles in response to graded painful skin and muscle stimulation. Brain Topogr. 13, 43–58.
Strick, P.L., Dum, R.P., Picard, N., 1998. Motor areas on the medial wall of the hemisphere. Novartis Found. Symp. 218 (64–75), 104–108 (discussion 75–80).
Svensson, P., Beydoun, A., Morrow, T.J., Casey, K.L., 1997. Non-painful and painful stimulation of human skin and muscle: analysis of cerebral evoked potentials. Electroencephalogr. Clin. Neurophysiol. 104, 343–350.
Talairach, J., Tournoux, P., 1988. Co-planar stereotaxic atlas of the human brain. Thieme Medical Publishers, New York.
Tanji, J., 1996. New concepts of the supplementary motor area. Curr. Opin. Neurobiol. 6, 782–787.
Torquati, K., Pizzella, V., Della Penna, S., Franciotti, R., Babiloni, C., Rossini, P.M., Romani, G.L., 2002. Comparison between SI and SII responses as a function of stimulus intensity. NeuroReport 13, 813–819.
Valeriani, M., Le Pera, D., Niddam, D., Arendt-Nielsen, L., Chen, A.C., 2000. Dipolar source modeling of somatosensory evoked potentials to painful and nonpainful median nerve stimulation. Muscle Nerve 23, 1194–1203.
Vogt, B.A., Pandya, D.N., 1987. Cingulate cortex of the rhesus monkey: II. Cortical afferents. J. Comp. Neurol. 262, 271–289.
Vogt, B.A., Vogt, L., 2003. Cytology of human dorsal midcingulate and supplementary motor cortices. J. Chem. Neuroanat. 26, 301–309.
Waberski, T.D., Gobbele, R., Darvas, F., Schmitz, S., Buchner, H., 2002. Spatiotemporal imaging of electrical activity related to attention to somatosensory stimulation. NeuroImage 17, 1347–1357.
Whittingstall, K., Stroink, G., Gates, L., Connolly, J.F., Finley, A., 2003. Effects of dipole position, orientation and noise on the accuracy of EEG source localization. Biomed. Eng. Online 2, 14.
Xiang, J., Hoshiyama, M., Koyama, S., Kaneoke, Y., Suzuki, H., Watanabe, S., Naka, D., Kakigi, R., 1997. Somatosensory evoked magnetic fields following passive finger movement. Brain Res. Cogn. Brain Res. 6, 73–82.
Yamasaki, H., Kakigi, R., Watanabe, S., Hoshiyama, M., 2000. Effects of distraction on pain-related somatosensory evoked magnetic fields and potentials following painful electrical stimulation. Brain Res. Cogn. Brain Res. 9, 165–175.